JACS
JOURNAL OF THE AMERICAN CHEMICAL SOCIETY

Article

Studies of the Mechanism and Origins of Enantioselectivity for the Chiral Phosphoric Acid-Catalyzed Stereoselective Spi-roketalization Reactions

Yaroslav Ya Khomutnyk, Alonso J. Arguelles, Grace A. Winschel, Zhankui Sun, Paul M. Zimmerman, and Pavel Nagorny

J. Am. Chem. Soc., **Just Accepted Manuscript** • DOI: 10.1021/jacs.5b12528 • Publication Date (Web): 07 Dec 2015

ACS Publications

Journal of the American Chemical Society is published by the American Chemical Society. 1155 Sixteenth Street N.W., Washington, DC 20036

Studies of the Mechanism and Origins of Enantioselectivity for the Chiral Phosphoric Acid-Catalyzed Stereoselective Spiroketalization Reactions

Yaroslav Ya. Khomutnyk, Alonso J. Argüelles, Grace A. Winschel, Zhankui Sun, Paul M. Zimmerman* and Pavel Nagorny*

Department of Chemistry, University of Michigan, 930 N. University Avenue, Ann Arbor, MI 48109

Spiroketalization, Acetalization, Chiral Phosphoric Acids, Brønsted Acid Catalysis, Mechanism, Computational Studies

ABSTRACT: Mechanistic and computational studies were conducted to elucidate the mechanism and the origins of enantiocontrol for the asymmetric chiral phosphoric acid-catalyzed spiroketalization reactions. These studies were designed to differentiate between the S_N1-like, S_N2-like and covalent phosphate intermediate-based mechanisms. The chiral phosphoric acid-catalyzed spiroketalization of deuterium-labeled cyclic enol ethers revealed a highly diastereoselective *syn*-selective protonation/nucleophile addition thus ruling out long-lived oxocarbenium intermediates. Hammett analysis of the reaction kinetics revealed positive charge accumulation in the transition state ($\rho = -2.9$). A new computational reaction exploration method along with the dynamics simulations supported an asynchronous concerted mechanism with a relatively short-lived polar transition state (average lifetime = 519 ± 240 fs), which is consistent with the observed inverse KIE = 0.85. Based on these studies, a transition state model explaining the observed stereochemical outcome was proposed. This model prediced enantioselective formation of the observed enantiomer of the product in 92% ee, which matches the experimentally observed value.

INTRODUCTION

The transformations leading to formation of spiroketal (spiroacetal) functionality represent a fundamentally important class of organic reactions, discussion of which can be found in the majority of the introductory organic chemistry textbooks.[1] A variety of natural products contain the spiroketal functionality, and the presence of such moiety is often crucial for their biological activity.[1-3] Spiroketalization leads to the formation of a new stereogenic center, and its configuration often defines the biological properties of the molecule (Figure 1). The molecules possessing only one stereogenic center arising from the spiroketal moiety are well documented, and the absolute configuration of such spiroketals may play an important role in determining the biological properties of these natural products. Thus, (*R*)-olean is a fruit fly sex pheromone that is known to act on male flies whereas its mirror image, (*S*)-olean affects female fruit fly.[2] Even in the cases when numerous additional stereocenters are present, the configuration of the spiroketal can be essential for the properties and biological activity of the molecule as it is the case for the cytotoxic natural product pectenotoxin 1, which was found to be more active than its thermodynamically more stable epimer, pectenotoxin 4.[3]

Numerous studies investigated factors governing the formation and stability of spiroketals. Typically, the stability of spiroketals is determined by both the steric and stereoelectronic effects, and in the absence of significant steric effects, stereoelectronic effects usually play the

Figure 1. Examples of natural products with challenging to synthesize spiroketals

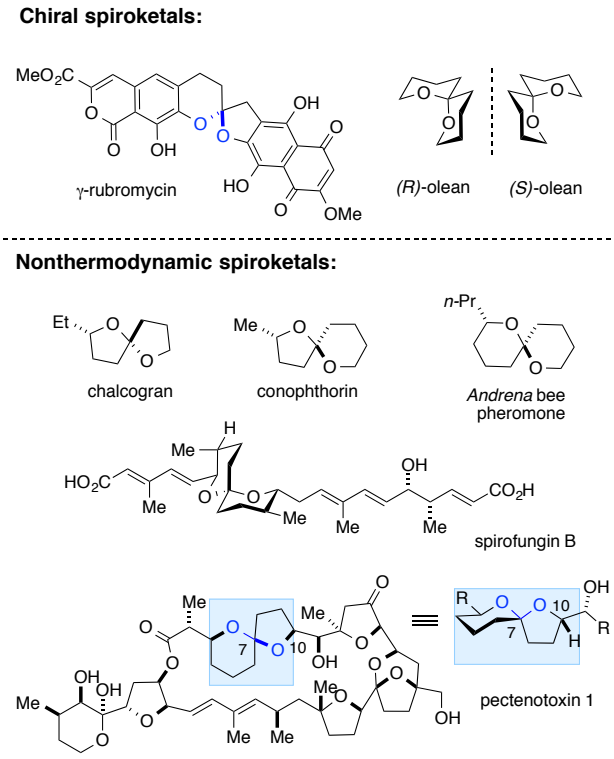

determining role.[4] The spiroketalization of dihydroxyketones (**1**, Scheme 1) may proceed through either hydroxyacetals **2** or cyclic enol ethers **3** and may lead to diastereomeric spiroketals **4** and **5**. Diastereomer **5** is more thermodynamically stable, and is typically the major product under equilibrating conditions. The preference for the formation of thermodynamic product **5** is attributed to stereoelectronic effect arising from an additional n(O)→σ*(C–O) stabilizing interaction, which is absent in the non-thermodynamic spiroketal **4**. The majority of natural spiroketals possesses thermodynamically-favored configurations, which leads to the assumption that their biosyntheses are under thermodynamic control. However, experimental evidence exists to suggest that spiroketal biosyntheses could also happen under enzymatic stereocontrol.[5]

Scheme 1.

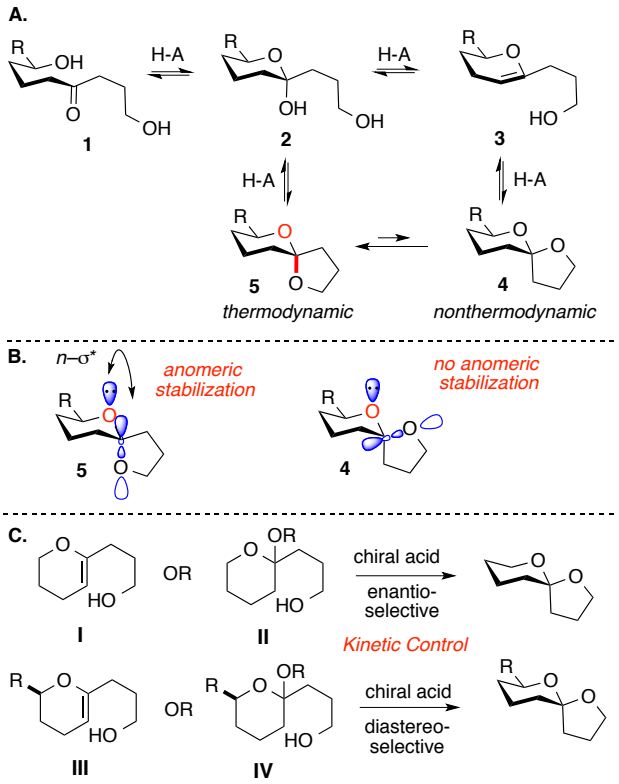

A. Formation of thermodynamic and nonthermodynamic spiroketals from dihydroxyketones (**1**) and cyclic enol ethers (**3**). B. Stereoelectronic stabilization of thermodynamic spiroketals. C. Catalyst-controlled spiroketalizations.

Considering that natural spiroketals prevalently possess the thermodynamically most stable configuration, the majority of synthetic approaches to natural spiroketals rely on catalyst-promoted cyclization under equilibrating conditions.[6,7] At the same time, similar conditions cannot be employed when a less stable nonthermodynamic configuration is desired (*cf.* pectenotoxin 1, Figure 1). In those cases, the stereoselective synthesis of spiroketals via direct acetalization becomes significantly more challenging.[8] Equally challenging is the enantioselective synthesis of a spiroketal moiety, in which case the ketal stereocenter is the only source of chirality in the natural product (*cf.* γ-rubromycin or olean, Figure 1). Most current approaches to non-thermodynamic or chiral spiroketals rely on substrate- or auxiliary-directed methods to form the spiroketal stereocenter.[8–10] The chiral reagent-controlled formations of spiroketals are also known, but significantly more rare.[10c] While the direct chiral catalyst-controlled formation of chiral and non-thermodynamic spiroketals would address the problems specified above, until recently, such transformations[11] as well as the catalyst-controlled formation of *O,O*-acetals[12] had been unknown. Among the various challenges associated with the use of chiral catalysts, promoting the formation of spiroketals without epimerization of the formed stereocenter and controlling the reactivity of the oxocarbenium ion intermediates could be highlighted as the major challenges to overcome. Our group has long-standing interests in hydrogen bond-donor catalysis and its applications to acetalization reactions.[11b,c,12g,13] Contemporaneously with the List and Coric,[11a] our group[11b] recently demonstrated that both of these problems could be avoided if chiral phosphoric acids are employed as the catalysts for the cycloisomerization of cyclic enol ethers **I** and **III** under the kinetic control. Correspondingly, this article summarizes our work on chiral phosphoric acid-catalyzed stereoselective spiroketalizations that could be used to synthesize chiral and nonthermodynamic spiroketal motifs (Figure 1). In addition, this article describes the experimental and computational studies directed to elucidate the mechanism and the origins of enantiocontrol for these reactions. Considering that many different mechanistic pathways can be proposed for these transformations, the described studies were designed to differentiate between these pathways and to gain information about the reactive intermediates. Thus, the cyclization of deuterated cyclic enol ethers, Hammett studies and secondary KIE studies were employed to differentiate between the S_N1-like, S_N2-like and covalent phosphate intermediate-based mechanisms. These studies suggest that the CPA-catalyzed cyclizations happen via polar concerted mechanism that does not involve long-lived oxocarbenium intermediates. A new computational reaction exploration method along with molecular dynamics computational studies independently validated this proposal and served to derive a transition state model explaining the observed stereochemical outcome.

RESULTS AND DISCUSSION

Initial optimization studies. Although CPAs had been previously employed to catalyze the formation of chiral *N,N*-,[14a-c,e] *N,O*-,[14d] *N,S*-,[14e,f] and simple *O,O*-acetals,[12] no examples of a successful chiral catalyst-controlled enantioselective or diastereoselective spiroketalization existed at the beginning of these studies. Despite these encouraging precedents, the prospects of using chiral Brønsted acids to promote catalyst-controlled spiroketalizations were unclear considering that spiroketals are significantly more prone to epimerization under acidic conditions. With this in mind, we surmised that the use of cyclic enol ethers **I** or **III** as the spirocyclization precursors was key in developing this transformation as the mixed acetal precursors **II** and **IV** (Scheme 1) are too

similar to spiroketals in their ability to ionize under the acidic conditions. The cycloisomerization of the enol ethers **I** and **III** is easier to achieve under the epimerization-free conditions, and the Deslongchamps and Pihko groups had previously utilized weak acids such as acetic acid (pKa = 4.7, H_2O) to promote kinetic spiroketalizations.[15] The same studies also indicate that the reactions catalyzed by stronger trifluoroacetic acid (pKa = –0.25, H_2O) proceeded under the thermodynamic control. At the same time, we surmised that the chiral phosphoric acids have intermediate acidities (pK_a ~ 2, H_2O), and would be excellent catalysts for kinetic spiroketalizations. In order to evaluate the feasibility of this proposal, spiroketalization of substrate **6a** into **8a** was investigated (Table 1).[11b] Commercially available (*S*)-TRIP (**7a**) was selected as the initial catalyst for the reaction optimization (Table 1); however, our subsequent attempts to identify a superior catalyst of this reaction were not successful (*cf.* Table S1 in SI).

Table 1. Initial evaluation of enantioselective spiroketalization reaction conditions

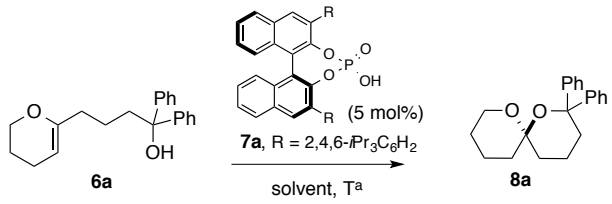

entry	solvent	T, °C	time,[b] h	conversion (yield), %	ee, %
1	CH_3CN	rt	0.5	100 (93)	7
2	THF	rt	12 [c]	30 (25)	10
3	EtOAc	rt	12	100 (98)	16
4	benzene	rt	1	100 (99)	24
5	toluene	rt	1	100 (98)	25
6	CCl_4	rt	1	100 (96)	40
7	hexanes	rt	0.5	100 (98)	63
8	cyclohexane	rt	0.5	100 (95)	60
9	pentane	rt	0.5	100 (97)	69
10	pentane	0	4	100 (97)	73
11	pentane	–35	40	100 (96)	66
12	pentane, 4 Å MS	0	14	100 (97)	84
13	**pentane, 4 Å MS**	**–35**	**40**	**100 (96)**	**92**

[a]Phosphoric acids were washed with 6 M HCl after the purification by the column chromatography. Unless specified otherwise, reactions were performed on 0.1 mmol scale (0.02 M solution). [b]Time required for the reactions to reach completion. [c]Incomplete conversion.

In our attempts to optimize the selectivity for the formation of **8a**, we have encountered significant solvent effects (Table 1). The reactions conducted in higher polarity solvents (entries 1–5) resulted in lower levels of stereocontrol while the oxygenated solvents such as THF and ethyl acetate significantly retarded the rate of cyclization (entries 2 and 3). At the same time, the spiroketalizations conducted in nonpolar hydrocarbon solvents (entries 7–9) proceeded with higher enantioselectivities and shorter reaction times. The observed solvent effects emphasize the significance of non-covalent interactions between the substrate and chiral phosphoric acid for the productive reaction pathway. More polar, oxygenated solvents (entries 2 and 3) can competitively form hydrogen bonds with CPA, and thus reduce the complexation with **6a**. At the same time, the less polar solvents favor enhanced hydrogen bonding and other types of non-covalent interactions between **6a** and **7a.** Based on these arguments, we surmised that the selectivity for the formation of **8a** can be further enhanced at lower reaction temperature and if the hydrogen-bonding impurities such as water are removed. Although lowering the reaction temperature alone did not significantly affect the enantioselectivity (entries 10 and 11), the addition of 4Å MS combined with lowering the temperature to –35 ºC resulted in the formation of **8a** in 92% ee (entry 12).

Table 2. Investigation of enantioselective spiroketalization substrate scope

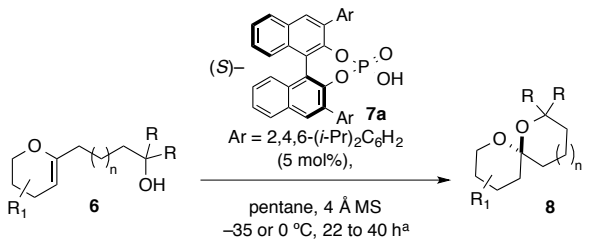

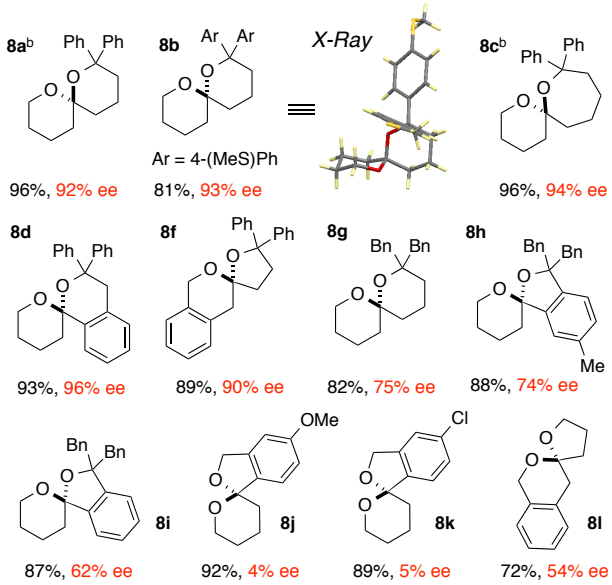

[a]Reactions were performed on 0.1–0.05 mmol scale (0.02 M solution), and the selectivities of these reactions were found to be scale independent. Catalyst (*R*)-**7a** was used. [b]Reactions were conducted with catalyst (*S*)-**7a**.

Enantioselective and Diastereoselective Spiroketalizations. After the optimal reaction conditions were identified, the scope of the enantioselective spiroketalization was evaluated next (Table 2). In addition to the previously evaluated **6a**, the cyclic enol ethers **6b–6l**

were synthesized and subjected to the cyclizations leading to **8b–8l**. The introduction of *p*-MeS- substituents at the aromatic rings of **6b** and extension of the tether length on **6c** did not affect the reaction yield and selectivity of **8b** and **8c**. Similarly, the introduction of a fused benzene ring into the side-chain (**8d**) or into the enol ether ring (**8e**) was well tolerated, and the corresponding products were obtained in excellent selectivities and yields. At the same time, the cyclization of analogous substrates **6g-6i** containing less rigid Bn– substituents at the tertiary alcohol consistently exhibited lower enantioselectivities. Cyclization leading to **8h** was found to be more selective (88%, 74% ee) than a similar reaction leading to **8i** that lacks a methyl group on the aromatic ring (87%, 62% ee). These results indicate that further variations in the substrate backbone can potentially enhance the selectivity of the substrates lacking Ph– substitution at the nucleophile. This is further reinforced by the observation that primary alcohol-containing precursor **6l** could be cyclized enantioselectively to **8l** (72%, 54% ee) while the reaction with a similar substrate **6j** and **6k** lead to almost unselective formation of spiroketals **8j** and **8k**.

Scheme 2. CPA-controlled formation of non-thermodynamic spiroketals

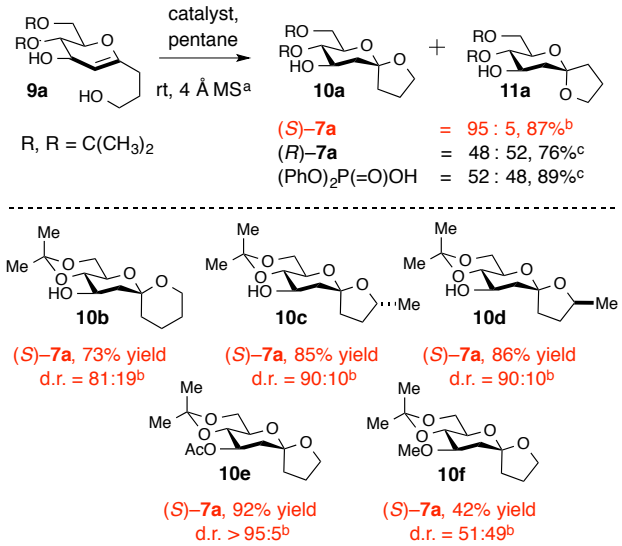

[a]The reactions with (*S*)-**2a** (5 mol%) and (*R*)-**2a** (5 mol%) were performed for 14 h and the reactions with $(PhO)_2PO_2H$ (10 mol%) were performed for 2 h. Longer exposure to $(PhO)_2PO_2H$ (10 mol%) resulted in complete equilibration to thermodynamic spiroketals. The cyclizations of **9a** were performed at different scales without significant variation in scale or selectivity. [b]Yield of non-thermodynamic spiroketal **10**. [c]Combined yield of **10** and **11**.

The results summarized in Table 2 indicate that chiral catalyst could control the selectivity of the cyclization of achiral substrates **6**. However, considering that the chirality of the substrate may completely override the course of cyclization dictated by the catalyst, the effect of the catalyst on the cyclization of chiral substrates had to be addressed next (Scheme 2).[11b] Since the reactions of carbohydrate-based oxocarbenium ions are highly sensitive to stereoelectronic and steric effects, the conformationally locked *D*-glucal derivatives (i.e. **9a**) were selected for these studies. Upon the spiroketalization, these substrates can provide anomerically stabilized thermodynamic products such as **11** or less stable nonthermodynamic spiroketals (**10a–10f**). Thus, to evaluate the effect of chiral catalyst on the course of these cyclizations, substrate **9a** was subjected to the treatment with (*S*)–**7a**, (*R*)–**7a**, as well as with achiral catalyst $(PhO)_2PO_2H$. Remarkably, the treatment of glycal **9a** with catalyst (*S*)-**7a** (5 mol%) resulted in a highly diastereoselective cyclization, leading to nonthermodynamic spiroketal **10a** (95:5 dr). At the same time, the exposure of **9a** to (*R*)-**7a** as well as to $(PhO)_2PO_2H$ provided ~1:1 mixtures of nonanomeric and anomeric products **10a** and **11a**, clearly indicating that the chirality of the catalyst is essential for the selective formation of **10a**. Similar trends were observed for other substrates, and catalyst (*S*)-**7a** was used for highly diastereoselective formation of various non-thermodynamic spiroketals (**10a–10e**) in good yields and diastereoselectivities. Interestingly, the nature of protecting group at C3 was found to play an important role, and unlike the formation of **10e**, the cyclization leading to **10f** was not selective.

The results summarized in Scheme 2 suggest that the cyclizations catalyzed by **7a** proceed under kinetic conditions. The nonanomeric spiroketals **10** are clearly stable to both enantiomers of acids **7a** for the duration of the reaction (i.e. 14 h). At the same time, if pure **10a** is treated with (*S*)-**7a** under the reaction conditions, a complete epimerization to **11a** was observed after 60 h.

Mechanistic Considerations. The results above suggest that **7a** is the catalyst of choice for the asymmetric spiroketalization of tertirary alcohol-containing substrates **6** as well as for the diastereoselective cyclization of chiral substrates **9** leading to nonanomeric spiroketals **10**. Interestingly, the larger size of glycals **9** excluded the requirement of using the tertiary alcohol-based nucleophiles and **7a** could promote the cyclizations leading to **10** with primary and secondary alcohols as nucleophiles in good-to-excellent selectivities. However, although the aforementioned results provide some crude idea about the scope and limitation of the method, the mechanistic and stereochemical models explaining the origins of the stereocontrol are essential for a more general use of these and related transformations.

Despite the fact that CPA-catalyzed transformations invoking oxocarbenium ion intermediates have received significant attention in the recent years, very few attempts to understand the mechanisms of such transformations and the factors governing the selectivity have been made.[16] The formation of stable oxocarbenium ion intermediates has been proposed in the recent computational studies of *N*-triflyl phosphoramide-catalyzed cyanohydrin ether formation[16a] and CPA-catalyzed Petasis-Ferrier rearrangements.[16b] However, instances when the theoretical studies identified alternative mechanisms not involving the formation of oxocarbenium ion intermediates have also been documented. Thus, the recent studies of the acid-catalyzed enantioselective formation of pyrrolidines by the Toste group[17] and piperidines by our groups[13d] identified alternative pathways involving covalently linked thiophosphate (or phosphate)

Scheme 3. Potential mechanism of CPA-catalyzed spiroketalizations

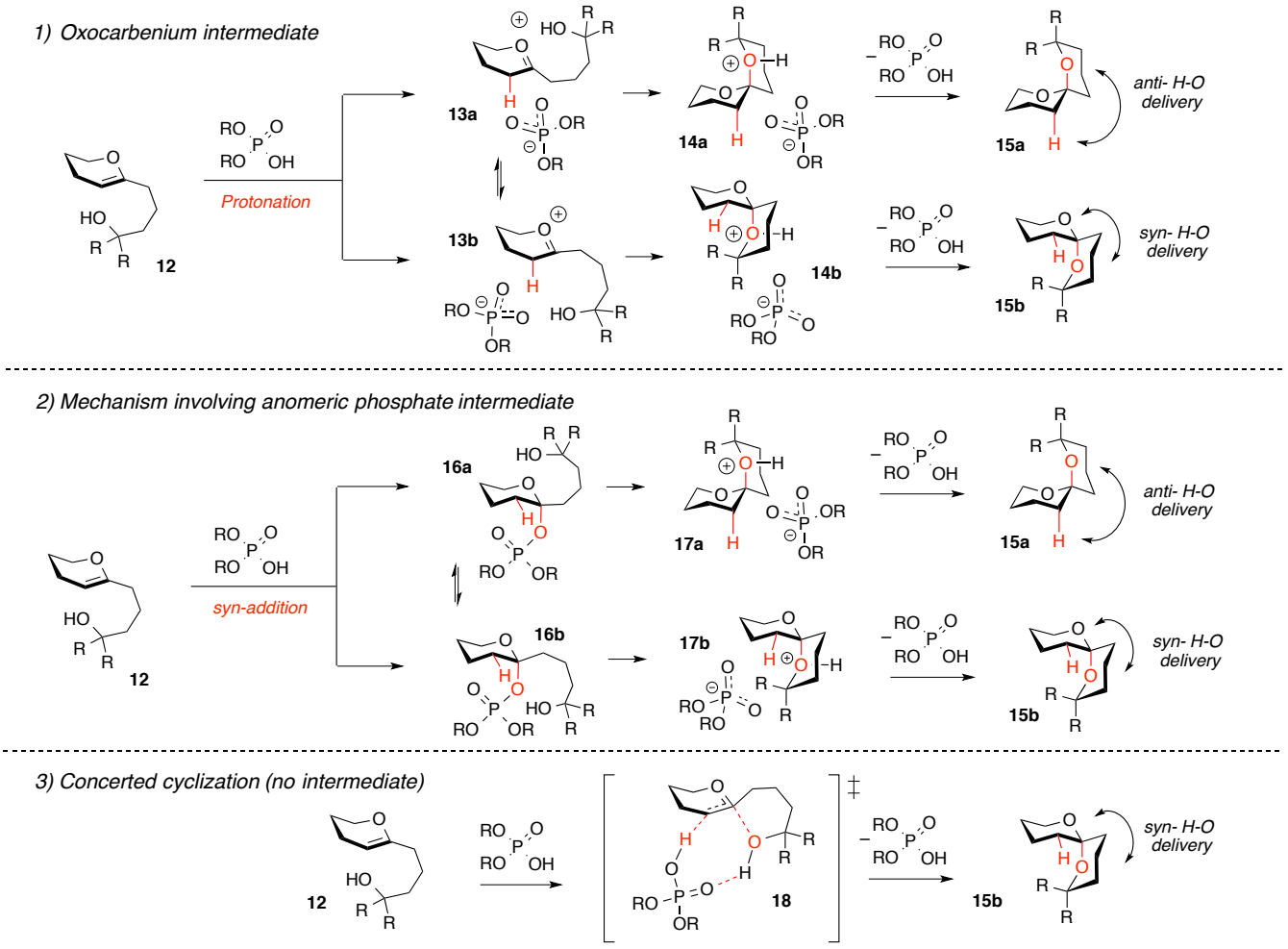

intermediates rather than the corresponding high-energy carbenium or oxocarbenium ion pairs. The oxocarbenium-based mechanisms for the acid-catalyzed acetal formation have indeed received widespread acceptance; however, transformations of this type not involving oxocarbenium ion intermediates have also been documented. Accordingly, the Tan group observed an S_N2-like concerted (rather than S_N1-like oxocarbenium-based) mechanism for the methanol-promoted spirocyclization of glycal epoxides.[18] In line with these findings is the theoretical study of the thiourea-catalyzed tetrahydropyranylation reaction by Schreiner and Kotke, in which a concerted asynchronous addition of alcohol nucleophiles rather than the formation of a discrete oxocarbenium ion intermediate is proposed.[19] Similarly, the true nature of the glycosylation reaction intermediates has been a subject of long-standing debates.[20] Both the ionic S_N1-like and concerted S_N2-like mechanisms are commonly invoked to explain the outcome of the glycosylation reactions, and there is strong evidence that non-ionic mechanisms are operational in some instances. For example, the Crich group has provided overwhelming evidence demonstrating that 4,6-O-benzylidene-directed β-mannosylation reactions proceed through covalently bound glycosyl triflates rather than through the discrete glycosyl oxocarbenium ion intermediates.[21]

With these prior observations in mind, we considered several different mechanistic pathways for the CPA-catalyzed enantioselective spiroketalization reaction (Scheme 3). The reaction mechanisms proceeding through oxocarbenium ion, covalently linked phosphate intermediate, and concerted mechanism with the concomitant C–H and C–O bond formation were viewed as the most prominent options. Both the counterion orientation and the relative stereochemistry of the forming C–H and C–O bonds are crucial for understanding the origins of stereoinduction and developing a stereochemical model. At the same time, these important factors are typically omitted from the mechanistic considerations. Thus, to our knowledge, no information on the selectivity of the C–H/C–O bond addition has been available prior to this work. In theory, the cyclization proceeding via an oxocarbenium ion intermediate can occur through two different modes. In the first mode of cyclization, the formation of the C–H and C–O bonds happen from the different faces of the molecule (i.e. pathway proceeding through **13a/14a/15a**). Alternatively, the pathway proceeding through **13b/14b/15b** and

resulting in *syn*- protonation/C–O bond formation can be envisioned. Similarly, the reaction proceeding through the anomeric phosphate intermediate conformations **16a** or **16b** can happen through the retentive or inversive (S_N2-like) mechanisms. The *anti*- relationship between the formed C–H and C–O bonds is expected for the inversive mechanism (i.e. **16a/17a/15a** pathway), and the *syn*- relationship between the formed C–H and C–O bonds is expected for the retentive mechanism (**16b/17b/15b** pathway). Unlike in the aforementioned mechanistic options that may lead to both the selective formation as well as mixtures of *syn*- and *anti*- products, the concerted mechanism, in which the phosphoric acid acts as the bifunctional catalyst, could produce only *syn*- product **15b** (Scheme 3).

Scheme 4. Diastereoselective spiroketalization of deuterium-labeled substrates

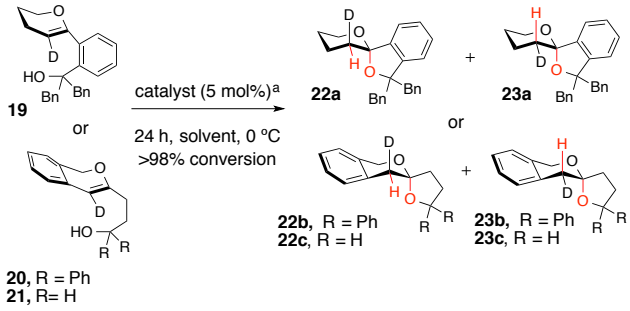

entry	catalyst	solvent	22a : 23a	22b : 23b	22c : 23c
1	*(S)*–**7a**	toluene	99 : 1	99 : 1	99 : 1
2	*(S)*–**7a**	CH_2Cl_2	99 : 1	99 : 1	99 : 1
3	*(S)*–**7a**	pentane	99 : 1	99 : 1	99 : 1
4	$ClCH_2CO_2H$[b]	pentane	99 : 1	99 : 1	99 : 1
5	$ClCH_2CO_2H$[b]	CH_2Cl_2	99 : 1	99 : 1	–[c]
6	*p*-TSA[d]	CH_2Cl_2	1 : 1	1 : 1	1 : 1
7	CF_3CO_2H[d]	pentane	1 : 1	1 : 1	1 : 1

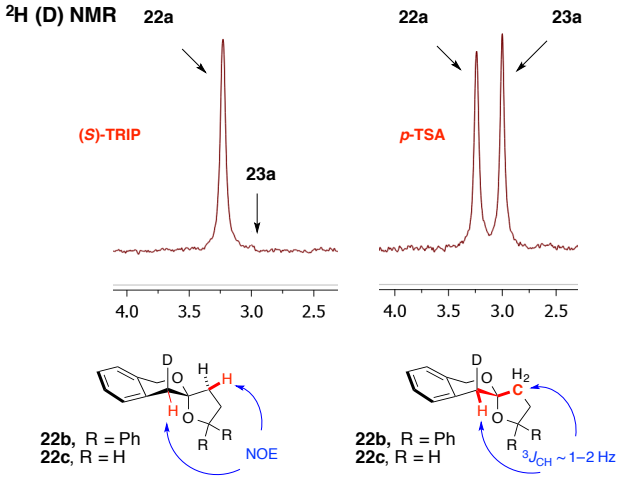

[a]The reactions were performed on 0.5–0.05 mmol scale, and each experiment was reproduced twice. D(^{2}H) NMR spectra were recorded at 107 MHz using Varian VNMRS-700. The observed diastereoselectivities were found to be conversion independent. [b]10 mol% of the catalyst was employed. [c]No reaction was observed. [d]The racemization reactions were found to be faster than the cyclization reactions under these conditions.

Diastereoselective Cyclizations Studies. With these considerations in mind, we designed and conducted experiments to distinguish between the diastereodivergent *syn*- or *anti*- spiroketalization modes (Scheme 4).

To obtain this information, we generated deuterated cyclic enol ethers **19–21** and subjected them to the cyclization in nonpolar solvents (i.e. toluene, dichloromethane and pentane) using (*S*)-**7a**, choroacetic acid, CF_3CO_2H or *p*-TSA as the catalysts. The outcome of these reactions was monitored using ^{2}H(D) NMR (107 MHz). As per our discussion above (i.e. Scheme 3), the cyclization of **19** may lead to *syn*- product **22a** or *anti*- product **23a**. Similarly, the cyclization of **20** or **21** may provide *syn*- diastereomers **22b** and **22c** or *anti*- diastereomers **23b** and **23c**, respectively. Remarkably, only *syn*- products **22a–c** were detected in the experiments with weaker acids (i.e. *(S)*-**7a** and $ClCH_2CO_2H$, entries 1–5); however, unselective formation of the *syn*- and *anti*- products was detected for the *p*-TSA catalyzed reactions (entries 6 and 7). The absence of the selectivity for the *p*-TSA catalyzed reactions is attributed to rapid epimerization under the cyclization conditions. Thus, subjecting diastereomerically pure **22b** to *p*-TSA at –40 ºC resulted in rapid isomerization to 1:1 mixture of **22b** and **23b** after 15 minutes. Finally, a substantial inverse kinetic isotope effect (KIE=0.85) was observed for the cyclization of **21c** into **22c** (*cf.* Eq. 1).

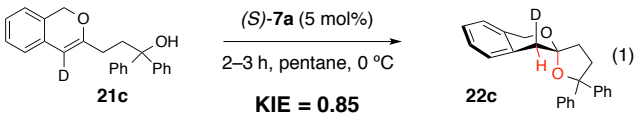

The relative configuration of **22a–22c** was established using NOE and 2D heteronuclear NMR studies, including $^3J_{CH}$ determination by SelEXSIDE,[22] and some of the key signals are depicted in Scheme 4 (*cf.* to Supporting information for additional details). Despite the numerous studies on the spiroketalization mechanism and the widespread use of spiroketals in organic synthesis, the results in Scheme 4 represent the first documented evidence suggesting that the kinetic spiroketalization of cyclic enol ethers in nonpolar solvents proceeds via highly selective *syn*- H/O addition. To investigate whether the *syn*- addition is more general and could be observed in intermolecular acetalization reactions, the reaction of *D*-labeled dihydropyrane (**24**) and *p*-methoxybenzyl alcohol was investigated next (Table 3). As for the spiroketalization studies with deuterium-labeled cyclic enol ethers, the formation of two diastereomeric products *syn*-**25a** and *anti*-**25b** is also expected in this case. The phosphoric acids (*S*)-**7a** and **26**, chloroacetic acid and Schreiner's thiourea **27** were selected as the catalysts.

The formation of **25** promoted by these catalysts is expected to be irreversible (i.e. kinetic) under most conditions since the THP-acetals possess significantly higher stability than typical spiroketals. Interestingly, tetrahydropyranylation reactions were found to be dissimilar to spiroketalization reactions.

Table 3. Acetalization with 3,4-dihydro-2*H*-pyran-5-*d*

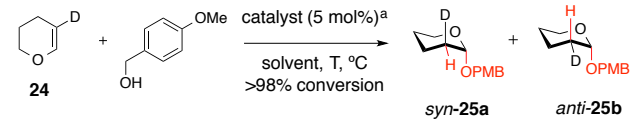

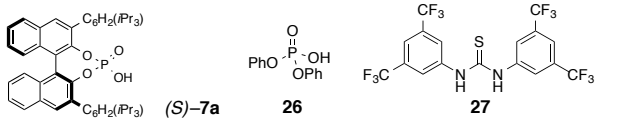

entry	catalyst	solvent	T, °C	time, h	*syn*-**25a** : *anti*-**25b**
1	*(S)*–**7a**	CH_2Cl_2	rt	12	1 : 1
2	**26**	pentane	0	48	1 : 1
3	**26**	benzene	rt	12	1 : 1
4[b]	$ClCH_2CO_2H$	neat	rt	48	–
5[c]	**27**	benzene	0	42	1 : 1

[a]The reactions with were performed at 0.15-0.59 mmol scale, and each experiment was reproduced twice. D(^{2}H) NMR spectra were recorded at 107 MHz on Varian 700. The observed diastereoselectivities were found to be conversion independent. [b]No reaction was observed with 10 mol% of the catalyst. [c]2 mol% of the catalyst **27** was employed.

Thus, the reaction of *p*-methoxybenzyl alcohol with **24** produced a ~1:1 mixture of products with Brønsted acids *(S)*-**7a** and **26** (entries 1–3), but no reaction was observed with chloroacetic acid (entry 4). Similar results were observed when unlabeled dihydropyrane was reacted with deuterium-enriched *p*-methoxybenzyl alcohol (**28**) using diphenylphosphoric acid **26** as the catalyst (Eq. 2).

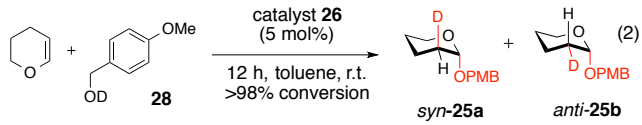

~1 : 1 mixture

As before, the nonselective formation of both *syn*- and *anti*- products was observed in this case. Tetrahydropyranylation of methanol catalyzed by thiourea catalyst **27** has been investigated computationally and the concerted asynchronous addition of methanol proceeding through a polar transition state with oxyanion hole stabilization by **27** has been proposed (*vide supra*).[19] Considering that a concerted asynchronous addition of alcohol to dihydropyrane **24** should result in the selective formation of *syn*-**25a**, we decided to investigate the outcome of the thiourea (**27**)-catalyzed formation of **25** (Table 3, entry 5). Surprisingly, thiourea (**27**)-catalyzed acetalization of **24** and *p*-methoxybenzyl alcohol produced an equimolar mixture of *syn*-**25a** and *anti*-**25b** in benzene. Since the formation of *syn*-**25a** and *anti*-**25b** is not reversible under the reaction conditions, the outcome of the experiments in Table 3 is consistent with the formation of a relatively long-lived, solvent-separated (rather than contact), oxocarbenium/stabilized alkoxide ion pair. This ion pair could undergo a non-selective association, and both faces of oxocarbenium ion are equally exposed to the reaction with the oxyanion nucleophile.

Figure 2. Hammett analysis of $(PhO)_2PO_2H$-catalyzed spiroketalization of **29**.

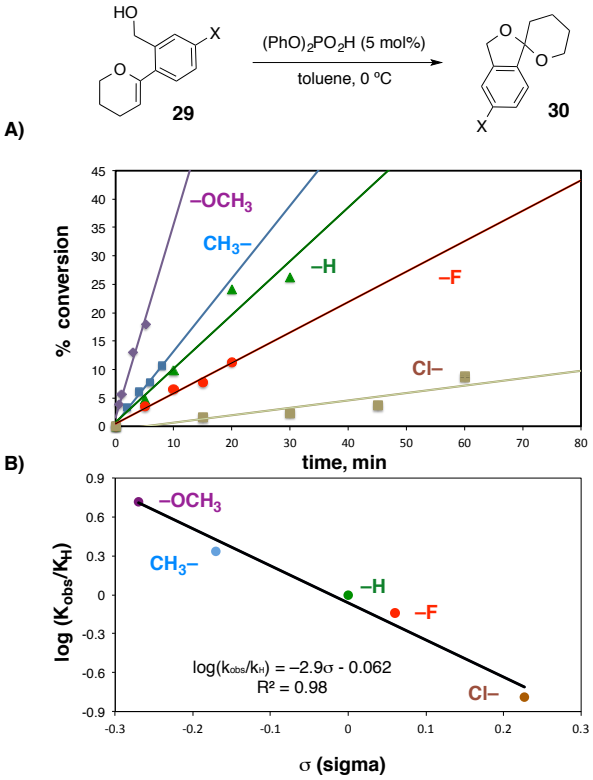

(A) Rates of conversion with of **29** with $(PhO)_2PO_2H$ (10 mol%) in toluene at 0 ºC. (B) Hammett plot exhibits a linear correlation for the electronically varied substrates **29** ($\rho = -2.9$).

Hammett Studies. The results above indicate that the intramolecular and intermolecular acetalization reactions proceed through different mechanisms. To further differentiate between the outlined in Scheme 3 mechanistic options, a Hammett study was executed for the cyclization of aromatic enol ether **29** leading to spiroketals **30** (Figure 2). Thus, the rate constants for the cyclization of substrates **29** with both electronwithdrawing (i.e. X = Cl–, F–) and electrondonating (i.e. X = CH_3O– and CH_3–) substituents as well as the unsubstituted substrate (X = H–) were measured at low conversions (Figure 2, A). The obtained $\log(K_{obs}/K_H)$ values for the electronically varied substrates **29** displayed an excellent linear correlation when plotted against the corresponding known σ values ($R^2 = 0.98$). These results allowed for the measurement of ρ value to be –2.9, which is consistent with a positive charge build up in the transition state of the rate-limiting step ($\rho < -1$). It should be noted that the obtained ρ value is lower than the one expected for an S_N1-like mechanism involving rate-limiting formation of fully charged oxocarbenium ion intermediate. In this regard, the Tan group has investigated the acid-catalyzed epimerization of kinetic *D*-glucal-derived spiroketals structurally similar to **29** and obtained $\rho = -5.1$, which is more in line with a rate-limiting ionization step than the ρ value obtained in these studies.

The results of the aforementioned studies shed some light on the mechanism of the CPA-catalyzed spiroketalization reactions. Thus, the observed highly diastereoselective *syn*- H–O delivery, a significant inverse KIE = 0.85 for

substrate **21c** (Eq. 1) indicating that re-hybridization happens in the rate-limiting step, and positive charge accumulation in the TS of the rate-limiting step observed in the Hammett study all speak against the formation of the covalent anomeric phosphate intermediates **16** (Scheme 3). These is further reinforced by the fact that *syn*- H–O delivery is observed not only for the phosphoric acid catalysts, but also for the chloroacetic acid. The relatively small ρ value and diastereoselective *syn*- H–O delivery are also not consistent with the long-lived oxocarbenium ion intermediates **13**, but more in accord with a highly asynchronous concerted mechanism proceeding through the polarized TS **18** (Scheme 3). At the same time, the scenaria with the formation of short-lived oxocarbenium/phosphate contact ion pair **13b** or phosphate **16** cannot be completely ruled out with the obtained experimental data. These distinctions, however, can be done based on the DFT calculations and molecular dynamics studies that would help to identify a pathway with the lowest energy and provide information on the average lifetime of the TS or intermediate involved. With these considerations in mind we undertook studies described in the next section.

Computational Studies. Asymmetric spiroketalization with chiral phosphoric acids may proceed through one or more of the mechanisms depicted in Scheme 3, of which the most classical one is mediated by an oxocarbenium intermediate. Experimental analysis of the mechanism provided strong evidence against *anti*-H-O delivery (to yield **15a**), but the mechanisms resulting in **15b** could not be ruled out. To gain further insight on the mechanism, the transformation was studied in depth using quantum chemical calculations.

Reactions mechanisms in relatively large systems with many flexible degrees of freedom-such as the present catalytic system-are especially difficult to characterize using reaction path optimization tools. To overcome these challenging cases, the Zimmerman group developed the Growing String Method (GSM) to simultaneously search for reaction paths and transition states.[23a,c,d] By restricting the search to find a transition state within a series of structures along a minimum energy path from reactant to product, GSM can efficiently locate transition states on highly flat energy surfaces. When our tools were applied to the asymmetric CPA-catalyzed formation of piperidines, an accurate description of the reaction selectivity was obtained, which invoked a two-step mechanism proceeding through a chiral phosphate acetal intermediate.[13d] In the piperidine formation mechanism and the present spiroketalization, GSM is especially useful in locating challenging asynchronous and concerted transformations due to its flexible treatment of the reaction pathway tangent vector (see Computational Details). Prior to the use of GSM to locate reaction pathways, a preliminary study of the diphenyl hydrogen phosphate-catalyzed spiroketalization of a simplified enol ether leading to 1,7-dioxaspiro[5.5]undecane was performed using the Zimmerman group's combinatorial reaction discovery procedure.[23b,e] The results suggested that the concerted pathway could compete with the phosphate-mediate and S_N1-like mechanisms.

Figure 3. Concerted, asynchronous mechanism for the ring closure of 6,6 spiroketalization model system.[a]

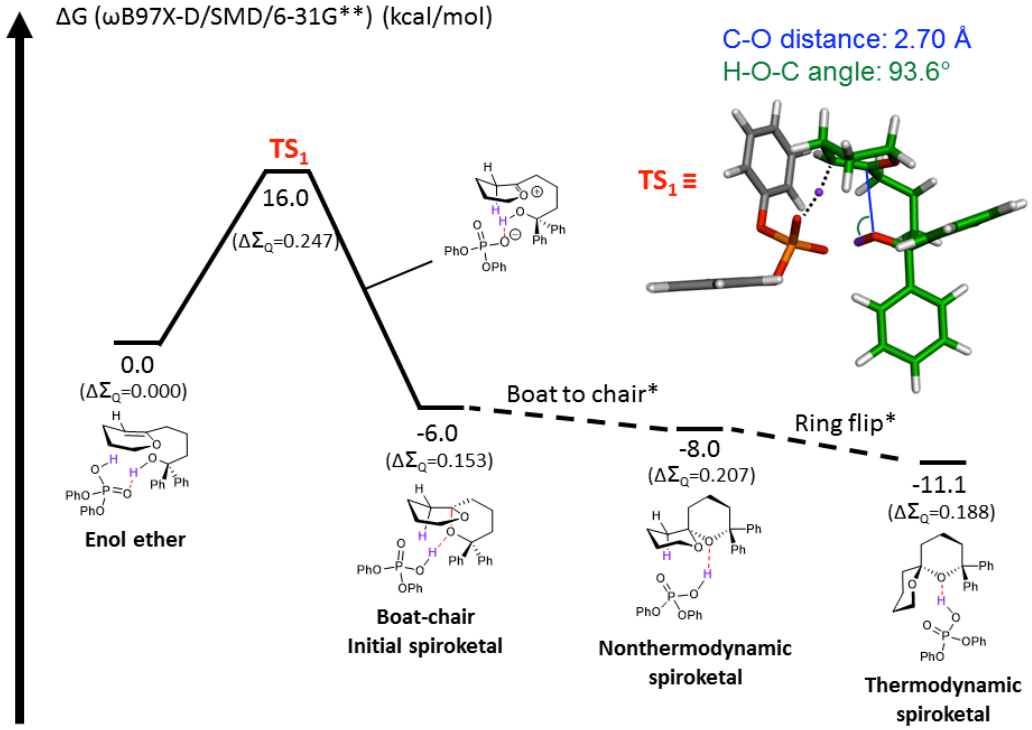

[a]The values in parenthesis correspond to the difference of the sum of Mulliken charges in the enol ether oxygen and electrophilic carbon with respect to the starting complex. *Barriers not calculated.

Figure 4. Anomeric phosphate mechanism of the 6,6 spiroketalization model system.[a]

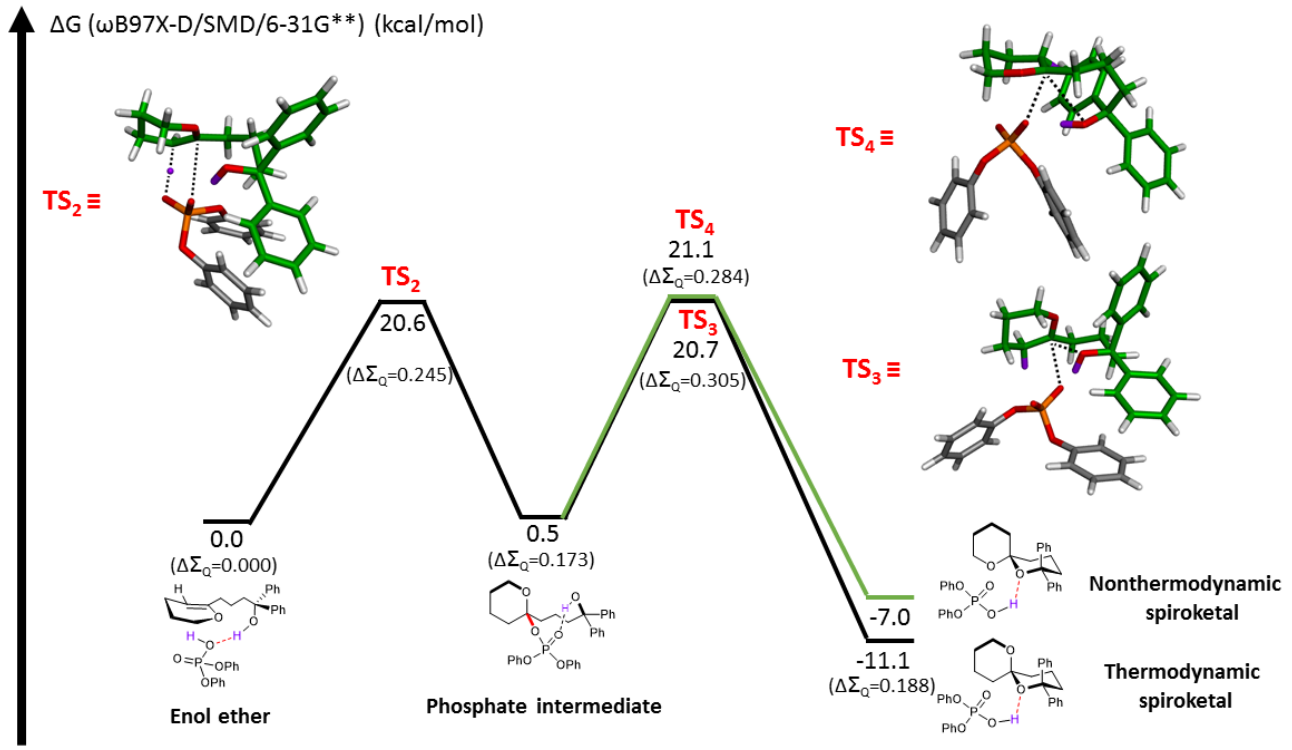

[a]The energy of important stationary points are shown in kcal/mol. The values in parenthesis correspond to the difference of the sum of Mulliken charges in the enol ether oxygen and electrophilic carbon with respect to the starting complex.

Following these preliminary results, more rigorous studies were performed which involved an initial extensive exploration of possible orientations of the catalyst-product complex for three different systems: the diphenyl phosphoric acid **26**-catalyzed 6,6-spiroketalization, the **26**-catalyzed 6,5-spiroketalization, and the chiral CPA **7a**-catalyzed 6,6-spiroketalization. Reaction path exploration and exact transition state searches were performed using GSM for each of the three types of mechanisms shown in Scheme 3. The resultant intermediates and transition states were corrected for thermodynamics and solvent effects (pentane). Reported energies are solvent-phase free energies with thermodynamic corrections at 298K (diphenyl hydrogen phosphate catalyst system) and 238K (**7a** catalyst system) from ωB97X-D/SMD/6-31G**.

To discriminate between the three mechanisms of Scheme 3, the transformation leading to a 6,6-spiroketal (substrate **6a**) was investigated first using a model diphenyl hydrogen phosphate catalyst. While this initial study did not use a chiral catalyst, the lowest barrier pathway unveiled by these simulations was further examined with the full catalyst (*vide infra*). Before examining the phosphate mediated and oxocarbenium pathways, 12 concerted pathways leading to thermodynamic and nonthermodynamic spiroketals were investigated. The most favored pathway produces a nonthermodynamic spiroketal (only one anomeric effect present) that can readily convert to the more stable thermodynamic spiroketal, as shown in Figure 3. The reaction pathway is concerted and asynchronous: from the substrate alcohol to phosphate H-bonded complex, an initial protonation of the enol ether occurs at the transition state (**TS₁**). Additionally, the transition state shows a chair-like geometry involving the alcohol oxygen and the electrophilic carbon, with a C-O distance of 2.70 Å. After the transition state, synchronous deprotonation and cyclization occurs. The initial spiroketal is formed in a chair-boat conformation, which can readily rearrange to a more stable nonthermodynamic chair-chair conformation and ultimately, by a ring flip, to the most thermodynamically stable spiroketal. The Mulliken charges on the enol ether oxygen and electrophilic carbon (provided in Figure 3) show a significant build-up of positive charge at **TS₁** ($\Delta\Sigma_Q$=0.247), slightly smaller than the sum of charges of a bare oxocarbenium solvated in *n*-pentane ($\Delta\Sigma_Q$=0.271, *cf.* SI). The activation barrier for this transformation was 16.0 kcal/mol above to the catalyst-substrate complex, fully consistent with a mechanism operative at or below room temperature. It should be noted that the dual function of the phosphoric acid as both Brønsted acid and Lewis base is efficiently exploited in this mechanism, as evident in the rate determining TS shown in Figure 3. Although the product initially formed is predicted to be the nonthermodynamic spiroketal, this is only relevant in conformationally locked systems such as the glucal derivatives shown in Scheme 2, since otherwise the thermodynamic spiroketal is readily accessed by a ring-flip.

The anomeric phosphate-mediated pathway was also examined using the diphenyl catalyst model system, and

different orientations of the catalyst were explored for this mechanism. The attack of each phosphate oxygen was examined, and the lowest energy pathway relevant to this mechanism is depicted in Figure 4. The initial orientation of the catalyst is similar to the concerted pathway described above, but the alcohol is not positioned such that ring-closure can readily occur. The formation of the anomeric phosphate intermediate instead proceeds through a concerted asynchronous mechanism. As initial protonation of the enol ether creates an ionic transition state, and since the alcohol moiety is further away from the electrophilic site, attack of the hydrogen-bonded oxygen of the phosphate can form an axial bond. The formation of the phosphate intermediate has a 20.6 kcal/mol barrier (**TS₂**), and its *syn* displacement by the nucleophilic alcohol to afford the spiroketal has a barrier of 20.7 kcal/mol (**TS₃**, the *anti*-phosphate displacement likely involves more than one phosphate and was not modeled). Once the phosphate intermediate is formed, there is not a large preference to the immediate formation of a thermodynamic compared to a nonthermodynamic spiroketal. In fact, although Figure 4 shows the sequence for the formation of the thermodynamic spiroketal, the phosphate could collapse to form a nonthermodynamic spiroketal (**TS₄**) with a 21.1 kcal/mol barrier.

The difference of 4.6 kcal between the concerted and anomeric phosphate mechanisms suggests that the phosphate mechanism is uncompetitive. To determine whether the concerted mechanism was also operative for 5-membered ring formation, reactions leading to a 6,5-spiroketal (**21c**) were examined. The relevant stationary points of the PES are shown in the SI. Not surprisingly, the data shows the concerted mechanism (E_a = 13.8 kcal/mol) is favored over the anomeric phosphate path (E_a = 22.9 kcal/mol for spiroketal formation by *syn*- displacement of the phosphate intermediate). The build-up of positive charge on the substrate and the asynchronicity of the changes in bonding are similar to the 6,6-spiroketalization. Finally, the KIE=0.96, calculated for the concerted mechanism, was in qualitative agreement with the experimentally measured value (KIE=0.85).

The study of an oxocarbenium-mediated mechanism proved challenging because repeated efforts to optimize stationary points for oxocarbenium intermediates resulted in their collapse to the reactant or product structures. This observation, however, makes sense in light of the proposed concerted mechanism for spiroketalization, where the TS itself is ionic (oxocarbenium-like). Given that an unstable oxocarbenium-like structure is initially formed along the concerted path, we turned to molecular dynamics to quantify the lifetime of this structure. If a stable oxocarbenium intermediate were possible, it should form after protonation of the substrate and be identified by dynamics simulations following the protonation TS. Therefore trajectories were sampled using quasi-classical initial velocities starting at the concerted TS structure to accurately mimic experimental conditions (see Computational Details). By plotting the C-O distance against time for the product's new C-O connection, Figure 5A shows how most of the 100 MD runs proceed from the TS to the product. By removing the trajectories that recrossed to the reactant species, Figure 5B shows the progression of product-forming trajectories to the ring-closed structures. Of the 71 runs, which resulted in product, an average time of 519 fs was required to form the spiroketal. No persistent oxocarbenium species were formed in any of the trajectories, including 7 trajectories needed to be run to 1.5 ps in order to complete product formation. This short timeframe is consistent with the concerted asynchronous mechanism derived by GSM without a stable intermediate along the pathway. Additionally, the trajectories show that the alcohol deprotonation and ring closure occur synchronously, also in agreement with the reaction path from GSM. This occurs due to the activation of the alcohol by the Lewis basic anionic oxygen of the catalyst, which quenches the positive charge build-up on the alcohol oxygen by simultaneously deprotonating it while it forms the C-O bond.

Having established a concerted yet asynchronous mechanism for spiroketalization with the model diphenyl catalyst system, the reactions of substrate **6a** and chiral phosphoric acid **7a** were studied next. Specifically, formation of *(R)*-spiroketal was modeled to determine the key interactions dictating the stereoselectivity of the reaction. Analogous orientations of the catalyst in the diphenyl phosphoric acid system were considered. To our delight, we found a 1.5 kcal/mol difference between the lowest computed activation barriers of the *(R)*-**7a**-catalyzed concerted spirocyclization and the *(S)*-**7a**-catalyzed, with the *(S)*-catalyst chirality being favored (see Figure 6). Since the *(R)* spiroketal was the designated simulation product, this result is in agreement with the chirality of the product formed in the experiment. Using a temperature of 238 K, we proceeded to calculate the expected enantiomeric excess, which is given by

$$ee = \frac{\exp\left(\frac{\Delta G^{TS}}{RT}\right) - 1}{\exp\left(\frac{\Delta G^{TS}}{RT}\right) + 1}$$

where ΔG^{TS} is the energy gap, R is the gas constant, and T is the temperature in Kelvin. The computed enantiomeric excess is of 92%, which exactly matches the experimental result.[11b]

While this is a very promising result, it is only accurate because the intrinsic errors in quantum chemical simulation have largely cancelled one another out. This agreement, however, has been seen in other applications of quantum chemical methods to a number of stereoselective transformations.[24] The extensive study of the PES by careful sampling of the driving coordinates and the end points of the strings, which included 5 different approaches of the catalyst to produce either thermodynamic (2 axial C-O bonds) or nonthermodynamic (2 equatorial C-O bonds, and both combinations of 1 axial and 1 equatorial C-O bond) spiroketals as well as the fact that the comparison between the lowest energy pathways for each catalyst chirality gives the proper selectivity, gives us confidence in our method and results.

Figure 5. Results of the molecular dynamics calculations on the TS of the concerted pathway of the 6,6 spiroketalization of the model system.

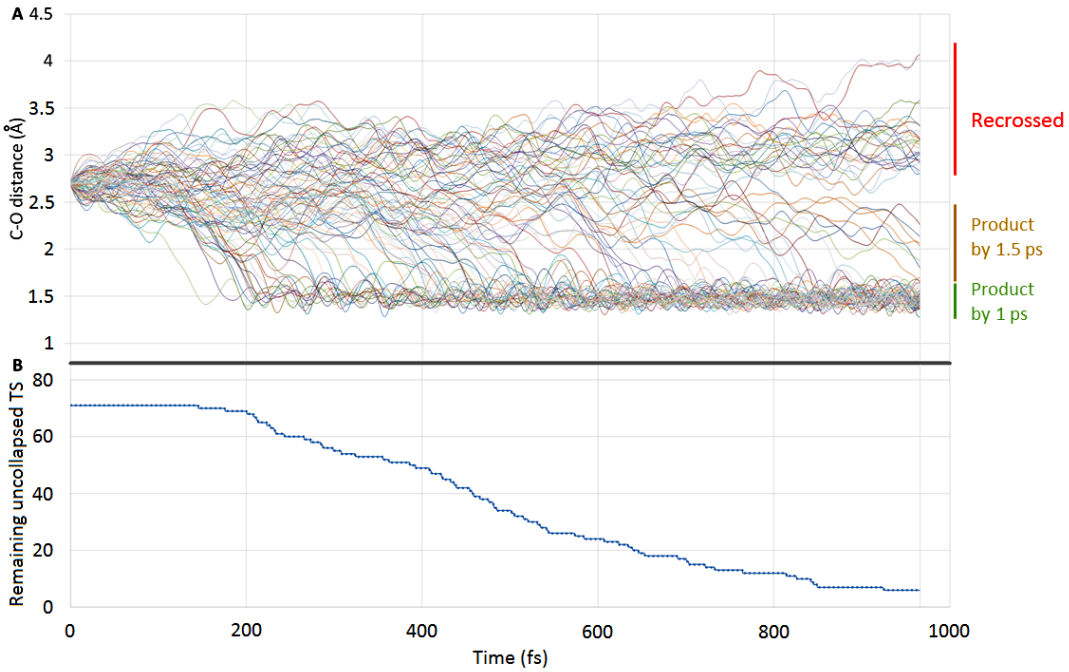

Each line represents one of the 100 independent runs. **A.** The new ring's C-O distance is plotted against time. **B.** The number of productive (71), but yet uncollapsed TSs is plotted against time.

Figure 6. Comparison of the activation barriers for the *(R)* and *(S)*-**7a** catalyzed spiroketalization.[a]

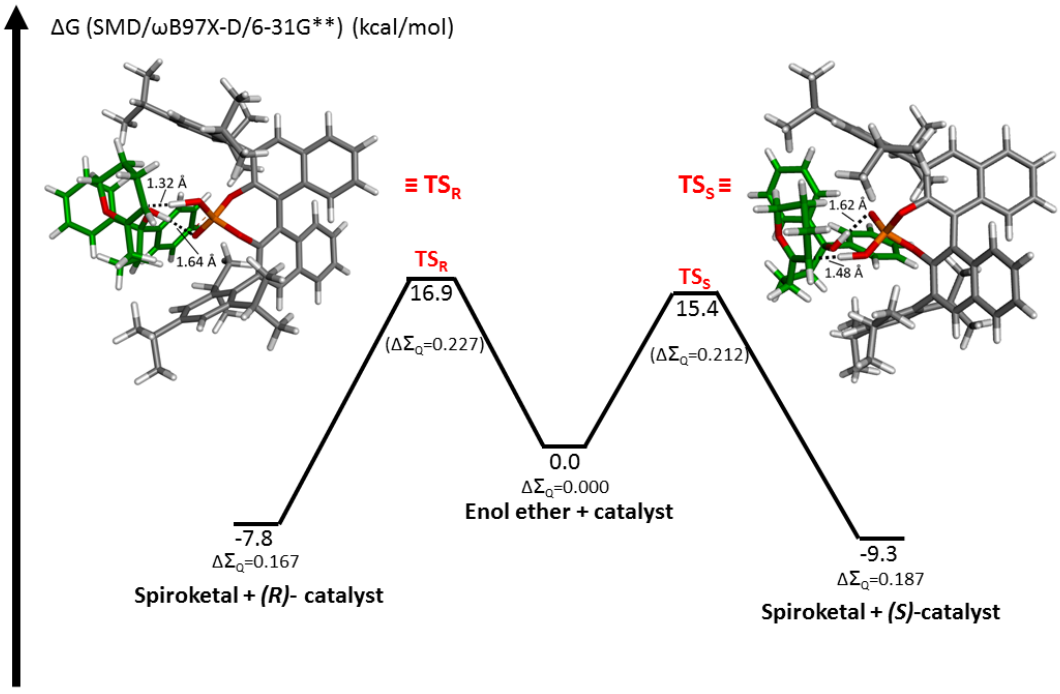

[a]The picture depicts the transition state structures. The values in parenthesis correspond to the difference of the sum of Mulliken charges in the enol ether oxygen and electrophilic carbon with respect to the starting complex.

Figure 7. Comparison of concerted asynchronous mechanism leading to the formation of a *(R)*-spiroketal involving *(S)*-**7a** ($\mathbf{TS_S}$) and *(R)*-**7a** ($\mathbf{TS_R}$).

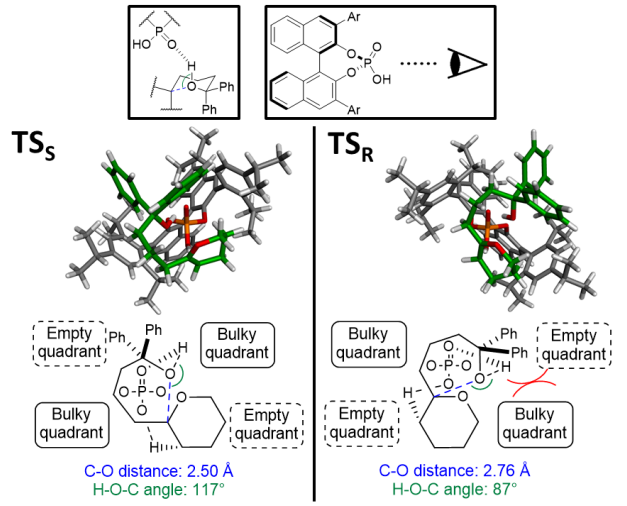

Figure 8. Key steric interactions at $\mathbf{TS_R}$ between the phenyl groups at the alcohol appendage of the enol ether and the ortho and para substituents of the aryl substituents of *(R)*-**7a**.

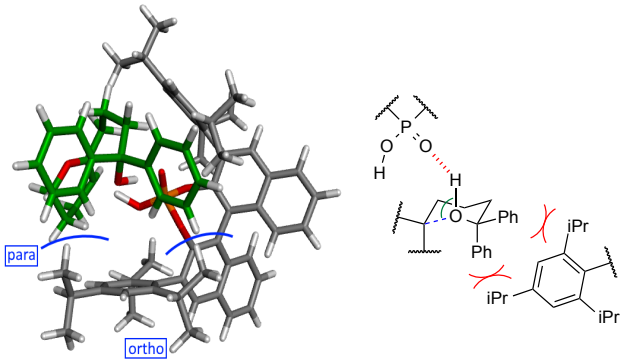

A description of the predicted mechanism and its associated stereochemical model follows. In the first step of the predicted concerted asynchronous mechanism, the catalyst, irrespective of its chirality, is initially oriented so that the phosphate oxygen hydrogen-bonds with the tertiary alcohol, while the Brønsted acidic hydrogen is aligned to add to the enol ether. As with the diphenyl catalyst model system, protonation of the enol ether occurs at the transition state for both catalyst chiralities. Also coherent with the diphenyl system, there is considerable build-up of positive charge on the substrate at the TS when compared to the enol ether-catalyst complex, in agreement with the experimental data on the mechanism (Hammet and SKIE experiments). For both catalyst chiralities, deprotonation of the nucleophilic oxygen and spirocyclization occurs simultaneously following protonation, as observed with diphenyl hydrogen phosphate model system. The cyclization occurs through a six-membered chair geometry to produce an initial boat-chair spiroketal, that initially relaxes to a nonthermodynamic spiroketal and finally, by means of a ring-flip, to the thermodynamic conformation. The relevant stationary points on the PES, disregarding the boat-chair spiroketal and the later isomerization to a thermodynamic product, are shown in Figure 6. While in this case the conformation of the immediately formed spiroketal is not vital (its equilibration to a more stable conformer is unimpeded), in conformationally locked structures it would be of importance. This mechanism shows how CPA catalysis can be used to form nonthermodynamic spiroketals with kinetic control. A major difference between the TS structures, which explains the kinetic origin of the enantioselectivity, is the interaction of the 2,4,6-triisopropylphenyl groups at the 3 and 3' position of **7a** with the phenyl rings of the tertiary alcohol of the substrate. Figure 7 shows the quadrant-based frontal perspective commonly used in stereochemical models involving CPAs and popularized by Himo[25] and Terada[26]. From this perspective, the diastereomeric relationship of the substrate-*(R)*-TRIP ($\mathbf{TS_R}$) and substrate-*(S)*-TRIP ($\mathbf{TS_S}$) spiroketalization TS is made clear. At the TS, the substrate is arranged in a way where protonation of the enol ether can take place, yet the positive charge being built in the electrophilic carbon is stabilized by its interaction with the alcohol oxygen. This is best achieved when the alcohol appendage adopts a chair-like geometry (Figure 7, top left diagram), in preparation for the asynchronous cyclization, and the phenyl rings are not located in the bulky quadrants near the catalytic site. To achieve this, the dihydropyran core is arranged in a different orientation for $\mathbf{TS_R}$ and $\mathbf{TS_S}$. The alcohol-containing side chain in $\mathbf{TS_R}$ adopts a less ideal chair-like geometry due to unfavorable steric interactions between the phenyl rings of the substrate and the ortho and para substituents at the aryl groups of the CPA. This is reflected by a longer distance between the nucleophilic oxygen and the electrophilic carbon (2.76 Å for $\mathbf{TS_R}$ and 2.50 Å for $\mathbf{TS_S}$) and a less directed angle for electronic interaction (87° H-O-C angle for $\mathbf{TS_R}$ and 117° for $\mathbf{TS_S}$). Figure 8 provides a perspective focusing on these key steric interactions in $\mathbf{TS_R}$. Substitution of the phenyl rings at the tertiary alcohol for more flexible benzyl groups is expected to relieve the steric congestion at $\mathbf{TS_R}$ and result in a decreased ee, as observed experimentally.

CONCLUSION

This article describes the development of chiral phosphoric acid-catalyzed stereoselective spiroketalizations as well as mechanistic and computational studies of the mechanistic origins of catalysis. The commercially available TRIP catalysts were found to be effective promoters of the enantioselective formation of chiral spiroketals and diastereoselective formation of nonanomeric spiroketals. The reactions were found to proceed under kinetic control, where nonpolar solvents (i.e. pentane) and anhydrous conditions (4 Å MS as additives) were found to be essential for attaining high levels of stereocontrol. The experimental studies were designed to differentiate between the S_N1-like, S_N2-like and covalent phosphate intermediate-based mechanisms. The chiral phosphoric

acid-catalyzed spiroketalization of deuterium-labeled cyclic enol ethers revealed a highly diastereoselective *syn*-selective protonation/nucleophile addition thus ruling out long-lived oxocarbenium intermediates. At the same time, the intermolecular equivalent of these reactions (i.e. tetrahydropyranylation with D3-labeled dihydropyrane) was found to proceed unselectively, presumably by a different (i.e. S_N1-like) mechanism. Hammett analysis of the reaction kinetics revealed positive charge accumulation in the transition state of the rate-limiting step ($r = -2.9$), and the KIE for the spiroketalization with D-labeled substrates was determined to be 0.85. The following in-depth computational studies on the phosphoric acid catalyzed spiroketalization mechanism suggest that a single step asynchronous mechanism is responsible for the observed experimental data. This mechanism fully exploits the bifunctionality of the catalyst and is novel for this type of transformations.[15] The anomeric phosphate pathway was shown to have higher energy barriers. Additionally, molecular dynamics simulations resulted in average lifetime of oxocarbenium structures average lifetime to be 519 ± 240 fs, which do not support stable ionic intermediate formation. The stereoselectivity of the reaction was examined in a complete system, and the key interactions which favor the experimentally observed results were identified to be linked with the 3,3` aryl substituents of the CPA and the substituents at the alcohol group of the substrate. This stereochemical model was highly consistent with the observed experimental results in terms of the selectivity and the levels of enantiocontrol, and his will allow the future catalyst design to overcome the procedure limitations and expand its scope, as well as the analysis of related reactions, such as intermolecular chiral phosphoric acid catalyzed acetal/aminal/hemiaminal ethers formation from enol ethers. Finally, the applicability of the growing string methods for the analysis of hydrogen-bond organocatalytic transformations involving large systems was demonstrated, as was its usefulness in the proposal of the underlying mechanism and in the explanation of the stereocontrol observed.

ASSOCIATED CONTENT

The experimental procedures, detailed description of computational studies, ^1H, ^2H and ^{13}C NMR spectra and HPLC traces are available free of charge via the Internet at http://pubs.acs.org.

AUTHOR INFORMATION

Corresponding Authors

*nagorny@umich.edu, paulzim@umich.edu

Funding Sources

This work has been supported by the National Science Foundation CAREER Award (CHE-1350060). PN is a Sloan Foundation and Amgen Young Investigator Fellow.

ACKNOWLEDGMENT

We thank Dr. Yong Guan for the help with the synthesis of substrates **20** and **21**. We also thank David Braun for computational support.

DEDICATION

We dedicate this paper to prof. James D. White on the occasion of his 80th birthday.

REFERENCES

1) (a) Perron, F.; Albizati, K. F. *Chem. Rev.* **1989**, *89*, 1616. (b) Mitsuhashi, S.; Shima, H.; Kawamura, T.; Kikuchi, K.; Oikawa, M.; Ichihara, A.; Oikawa, H. *Bioorg. Med. Chem. Lett.* **1999**, *9*, 2007. (c) Uckun, F. M.; Mao, C.; Vassilev, A. O.; Huang, H.; Jan, S.-T. *Bioorg. Med. Chem. Lett.* **2000**, *10*, 541. (d) Huang, H.; Mao, C.; Jan, S.-T.; Uckun, F. M. *Tetrahedron Lett.* **2000**, *41*, 1699.

2) Booth, Y. K.; Kitching, W.; De Voss, J. J. *Nat. Prod. Rep*. **2009**, *26*, 490.

3) Dominguez, H. J.; Paz, B.; Daranas, A. H.; Notre, M.; Franco, J. M.; Fernandez, J. J. *Toxicon* **2010**, *56*, 191.

4) Deslongchamps, P. *Stereoelectronic Effects in Organic Chemistry*, Pergamon Press Ltd. Oxford; **1983.**

5) (a) Gallimore, A. R.; Stark, C. B. W.; Bhatt, A.; Harvey, B. M.; Demydchuk, Y.; Bolanos-Garcia, V.; Fowler, D. J.; Staunton, J.; Leadlay, P. F.; Spencer, J. B. *Chem. Biol.* **2006**, *13*, 453; (b) Takahashi, S.; Toyoda, A.; Sekiyama, Y.; Takagi, H.; Nogawa, T.; Uramoto, M.; Suzuki, R.; Koshino, H.; Kumano, T.; Panthee, S.; Dairi, T.; Ishikawa, J.; Ikeda, H.; Sakaki, Y.; Osada, H. *Nat. Chem. Biol.* **2011**, *7*, 461.

6) (a) Boivin, T. L. B. *Tetrahedron* **1987**, *43*, 3309. (b) Mead, K. T.; Brewer, B. N. *Curr. Org. Chem.* **2003**, *7*, 227. (c) Raju, B. R.; Saikia, A. K. *Molecules* **2008**, *13*, 1942. (d) Sperry, J.; Liu, Y.-C.; Brimble, M. A. *Org. Biomol. Chem.* **2010**, *8*, 29. (e) Cala, L.; Fananas, F. J.; Rodriguez, F. *Org. Biomol. Chem*. **2014**, *12*, 5324.

7) (a) Aho, J. E.; Pihko, P. M.; Rissa, T. K. *Chem. Rev.* **2005**, *105*, 4406. (b) Favre, S.; Vogel, P.; Gerber-Lemaire, S. *Molecules* **2008**, *13*, 2570. (c) Sous, M. E.; Ganame, D.; Zanatta, S.; Rizzacasa, M. A. *ARKIVOC* **2006**, *vii*, 105.

8) For the overview of transition metal-catalyzed formation of spiroketals refer to: (a) Palmes, J. A.; Aponick, A. *Synthesis* **2012**, *44*, 3699.

9) For representative approaches to kinetic spiroketals refer to the following: (a) Pihko, P. M.; Aho, J. E. *Org. Lett.* **2004**, *6(21)*, 3849. (b) Takaoka, L. R.; Buckmelter, A. J.; LaCruz, T. E.; Rychnovsky, S. D. *J. Am. Chem. Soc*. **2005**, *127*, 528. (c) LaCruz, T. E.; Rychnovsky, S. D. *Org. Lett.* **2005**, *7(9)*, 1873. (d) Potuzak, J. S.; Moilanen, S. B.; Tan, D. S. *J. Am. Chem. Soc.* **2005**, *127*, 13796. (e) Moilanen, S. B.; Potuzak, J. S.; Tan, D. S. *J. Am. Chem. Soc.* **2006**, *128*, 1792. (f) Vellucci, D.; Rychnovsky, S. D. *Org. Lett.* **2007**, *9(4)*, 711. (g) Castagnolo, D.; Breuer, I.; Pihko, P. M. *J. Org. Chem.* **2007**, *72(26)*, 10081. (h) Liu, G.; Wurst, J. M.; Tan, D. S. *Org. Lett.* **2009**, *11(16)*, 3670. (i) Sharma, I.; Wurst, J. M.; Tan, D. S. *Org. Lett.* **2014**, *16*, 2474.

10) For representative auxiliary-based approaches to chiral spiroketals refer to following: (a) Iwata, C.; Hattori, K.; Uchida, S.; Imanishi, T. *Tetrahedron Lett.* **1984**, *25(28)*, 2995. (b) Iwata, C.; Fujita, M.; Hattori, K.; Uchida, S.; Imanishi, T. *Tetrahedron Lett.* **1985**, *26(18)*, 2221. (c) Uchiyama, M.; Oka, M.; Harai, S.; Ohta, A. *Tetrahedron Lett.* **2001**, *42(10)*, 1931. (d) Wu, K.-L.; Wilkinson, S.; Reich, N. O.; Pettus, T. R. R. *Org. Lett.* **2007**, *9(26)*, 5537. Aitken, H. R. M.; Furkert, D. R.; Hubert, J. G.; Wood, J. M.; Brimble, M. A. *Org. Biomol. Chem.* **2013**, *11*, 5147.

11) Catalyst-controlled asymmetric spiroketalization reactions: (a) Coric, I.; List, B. *Nature* **2012**, *483*, 315; (b) Sun, Z.; Winschel, G. A.; Borovika; Nagorny, P. A. *J. Am. Chem. Soc.* **2012**, *134*, 8074; (c) Nagorny, P.; Syn, Z.; Winschel, G. A. *Synlett* **2013**, *24*, 661. (d) Quach, R.; Furket, D. P.; Brimble, M. A. *Tetrahedron Lett.* **2013**, *54*, 5865. Wu, H.; He, Y.-P.; Gong, L.-Z. *Org. Lett.* **2013**, *15*, 460. (e) Wang, X.; Guo, P.; Wang, X.; Wang, Z.; Ding, K. L. *Adv. Synth. Catal.* **2013**, *355*, 2900. (f) Cala, L.; Mendoza, A.; Fananas, F. J.; Rodriguez, F. *Chem. Commun.* **2013**, *49*, 2715. (g) Wang, F.; Chen, F.; Qu, M.; Li, T.; Liu, Y.; Shi, M. *Chem. Commun.* **2013**, *49*, 3360. (h) Abulikemu, R.; Maihemuti, M. *Tetrahedron Lett.* **2015**, *56*, 2651.

12) Catalyst-controlled acetalization reactions: (a) Nagano, H.; Katsuki, T. *Chem. Lett.* **2002**, *8*, 782-783 (b) Coric, I.; Vellalath, S.; List, B. *J. Am. Chem. Soc.* **2010**, *132*, 8536-8537. (c) Coric, I.; Muller, S.; List, B. *J. Am. Chem. Soc.* **2010** *132*, 17370-17373. (d) Cox, D. J.; Smith, M. D.; Fairbanks, A. J. *Org. Lett.* **2010**, *12*, 1452. (e) Rubush, D. M.; Morges, M. A.; Rose, B. J.; Thamm, D. H.; Rovis, T. *J. Am. Chem. Soc.* **2012**, *134*, 13554. (f) Kim, J. H.; Coric, I.; Vellalah, S.; List, B. *Angew. Chem. Int. Ed.* **2013**, *52*, 4474. (g) Mensah, E.; Camasso, N.; Kaplan, W.; Nagorny, P. *Angew. Chem. Int. Ed.* **2013**, *52*, 12932; (h) Chen, Z.; Sun, J. *Angew. Chem. Int. Ed.* **2013**, *52*, 13593. (i) Kimura, T.; Sekine, M.; Takahashi, D.; Toshima, K. *Angew. Chem. Int. Ed.* **2013**, *52*, 12131. (j) Rubush, D. M.; Rovis, T. *Synlett* **2014**, *25*, 713. (k) Yamanaka, T.; Kondoh, Z.; Terada, M. *J. Am. Chem. Soc.* **2015**, *137*, 1048. (l) Kim, J. H.; Coric, I.; Palumbo, C.; List, B. *J. Am. Chem. Soc.* **2015**, *137*, 1778. (m) Matsumoto, A.; Asano, K.; Matsubara, S. *Chem. Commun.* **2015**, *51*, 11693. (n) Liyin, J.; Tao, J.; Min, W. *Org. Lett.* **2015**, *17*, 1070. (o) Quian, H.; Zhao, W.; Wang, Z.; Sun, J. *J. Am. Chem. Soc.* **2015**, *137*, 560.

13) (a) Borovika, A.; Nagorny, P. *Tetrahedron* **2013**, *69*; 5719. (b) Borovika, A.; Tang, P.-I.; Klapman, S.; Nagorny, P. *Angew. Chem. Int. Ed.* **2013**, *52*, 13424. (c) Bhattarai, B.; Tay, J.-H.; Nagorny, P. *Chem. Commun.* **2015**, *51*, 5398. (d) Sun, Z.; Winschel, G. A.; Zimmerman, P.; Nagorny, P. *Angew. Chem. Int. Ed.* **2014**, *53*, 11194. (e) Tay, J. H.; Arguelles, A. J.; Nagorny, P. *Org. Lett.* **2015**, 17, 3774.

14) (a) Rowland, G. B.; Zhang, H.; Rowland, E. B.; Chennamadhavuni, S.; Wang, Y.; Antilla, J. C. *J. Am. Chem. Soc.* **2005**, *127*, 15696-15697. (b) Liang, Y.; Rowland, E. B.; Rowland, G. B.; Perman, J. A.; Antilla, J. C. *Chem. Commun.* **2007**, 4477-4479. (c) Cheng, X.; Vellalath, S.; Goddard, R.; List, B. *J. Am. Chem. Soc.* **2008**, *130*, 15786-15787. (d) Li, G.; Fronczek, F. R.; Antilla, J. C. *J. Am. Chem. Soc.* **2008**, *130*, 12216-12217. (e) Rueping, M.; Antonchick, A. P.; Sugiono, E.; Grenader, K. *Angew. Chem. Int. Ed.* **2009**, *48*, 908-910. (f) Ingle, G. K.; Mormino, M. G.; Wojtas, L.; Antilla, J. C. *Org. Lett.* **2011**, *13(18)*, 4822-4825.

15) (a) Pothier, N.; Goldstein, S.; Deslongchamps, P. *Helv. Chim. Acta* **1992**, *75*, 604; (b) Castagnolo, D.; Breuer, I.; Pihko, P. M. *J. Org. Chem.* **2007**, *72*, 10081.

16) (a) Lu, C.; Su, X.; Floreancig, P. E. *J. Org. Chem.* **2013**, *78*, 9366; (b) Kanomata, K.; Toda, Y.; Shibata, Y.; Yamanaka, M.; Tsuzuki, S.; Gridnev, I. D.; Terada, M. *Chem. Sci.* **2014**, *5*, 3515.

17) Shapiro, N. D.; Rauniyar, V.; Hamilton, G. L.; Wu, J.; Toste, D. F. *Nature* **2011**, *470*, 245.

18) Wurst, J. M.; Liu, G.; Tan, D. S. *J. Am. Chem. Soc.* **2011**, *133*, 7916.

19) Kotke, M.; Schreiner, P. R. *Synthesis* **2007**, *5*, 779.

20) (a) Bohe, L.; Crich, D. *Carbohydr. Res.* **2015**, *403*, 48; (b) Crich, D. *Acc. Chem. Res.* **2010**, *43*, 1144; (c) Bohe, L.; Crich, D. *C. R. Chimie* **2011**, *14*, 3; (d) Beaver, M. G.; Billings, S. B.; Woerpel, K. A. *Eur. J. Org. Chem.* **2008**, 771; Smith, D. M.; Woerpel, K. A. *Org. Biomol. Chem.* **2006**, *4*, 1195; (e) Whitfield, D. M. *Adv. Carbohydr. Chem. Biochem.* **2009**, *62*, 83.

21) (a) Huang, M.; Garrett, G. E.; Birlirakis, N.; Bohe, L.; Pratt, D. A.; Crich, D. *Nature Chem.* **2012**, *4*, 663; (b) Huang, M.; Retaileau, P.; Bohe, L.; Crich, D. *J. Am. Chem. Soc.* **2012**, *134*, 14746; (c) Crich, D. Sharma, I. *J. Org. Chem.* **2010**, *75*, 8383; (d) Crich, D.; Vinogradova, O. *J. Org. Chem.* **2006**, *71*, 8473; (e) Crich, D.; Sun, S. *J. Am. Chem. Soc.* **1997**, *119*, 11217; (f) Crich, D.; Sun, S. *J. Org. Chem.* **1997**, *62*, 1198; (g) Crich, D.; Sun, S. *J. Org. Chem.* **1996**, *61*, 4506.

22) Butts, P. C.; Heise, B.: Tatolo, G. *Org. Lett.* **2012**, *14*, 3256.

23) (a) Zimmerman, P. M. *J. Comput. Chem.*, **2013**, *34* (16), 1385-1392. (b) Zimmerman, P. M. *J. Chem. Phys.* **2013**, *138*, 184102. (c) Zimmerman, P. M. *J. Chem. Theory Comput.* **2013**, *9* (7), 3043–3050. (d) Zimmerman, P.M. *J. Comput. Chem.* **2015**, *36*, 601–611. (e) Zimmerman, P. M. *Mol. Simul.* **2015**, 41(1-3), 43-54.

24) For selected applications of quantum chemical methods in the study of stereoselective organocatalytic reactions refer to (a) Allemann, C.; Gordillo, R.; Clemente, F. R.; Cheong, P. H. Y.; Houk, K. N. *Acc. Chem. Res.* **2004**, *37*, 558-569. (b) Markad, S. D.; Xia, S.; Snyder, N. L.; Surana, B.; Morton, M. D.; Hadad, C. M.; Peczuh, M. W. *J. Org. Chem.* **2008**, *73*, 6341-6354. (c) Schneebeli, S. T.; Hall, M. L.; Breslow, R.; Friesner, R. *J. Am. Chem. Soc.* **2009**, 131, 3965-3973. (d) Krenske, E. H.; Houk, K. N. *Acc. Chem. Res.* **2013**, *46* (4), 979-989.

25) Marcelli, T.; Hammar, P.; Himo, F. *Chem. Eur. J.* **2008**, *14*, 8562.

26) Gridnev, I. D.; Kouchi, M.; Sorimachi, K.; Terada, M. *Tetrahedron Lett.* **2007**, *48*, 497.

Insert Table of Contents artwork here